Toroidal and Slab ETG Dominance in the Linear Spectrum of JET-ILW Pedestals

Jason Parisi

with

Felix Parra, Colin Roach, Carine Giroud, Nobuyuki Aiba, Michael Barnes, Plamen Ivanov

University of Oxford, CCFE, JET, Rokkasho Fusion Institute

12th Plasma Kinetics Working Meeting

July 30 2019

Pedestal extends around $\overline{\psi} = 0.9 - 1.0$, $\overline{\psi} = \psi/\psi(\mathrm{LCFS})$.

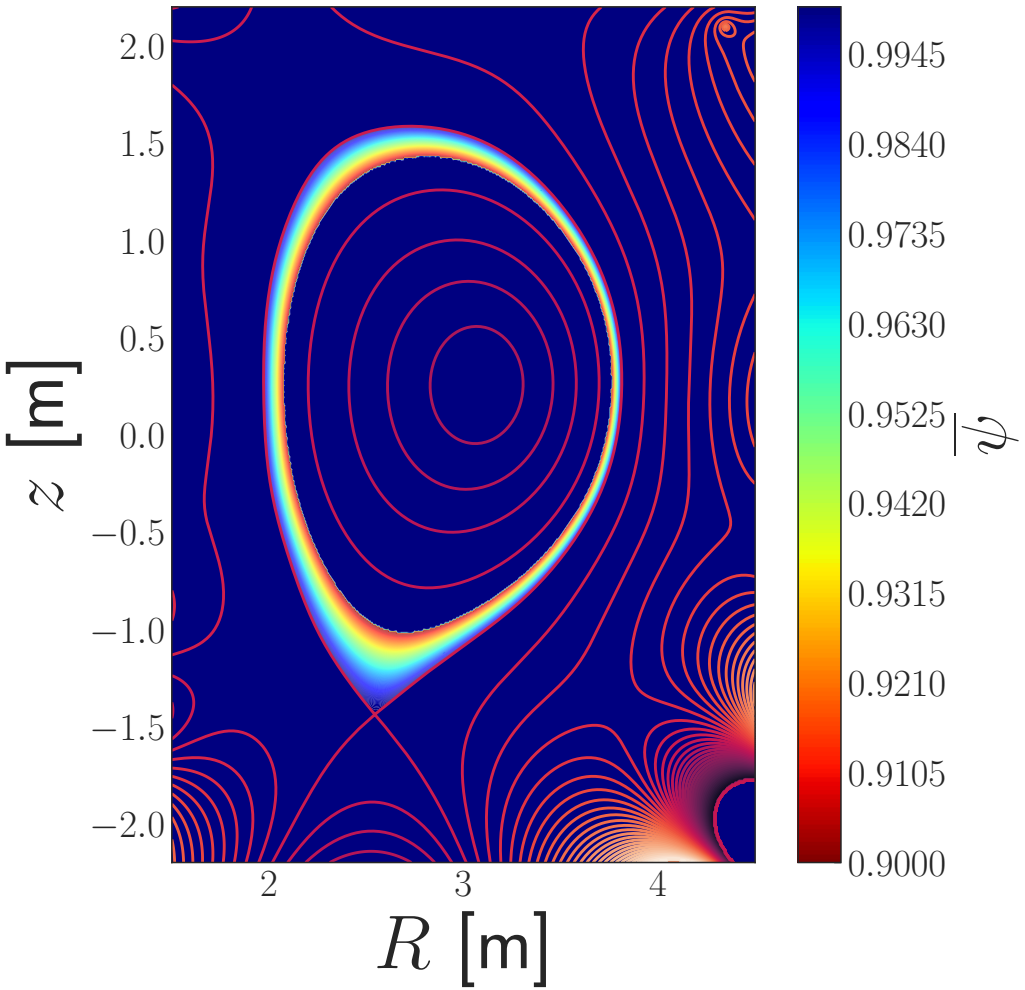

Figure: Surfaces of constant $\overline{\psi}$ for a JET-ILW discharge 92174. Pedestal region is highlighted.

Equilibrium pedestal profiles are very steep in the pedestal.

⇒ expect microinstabilities to be strongly driven.

- Measured T_i flatter than T_e in pedestal.

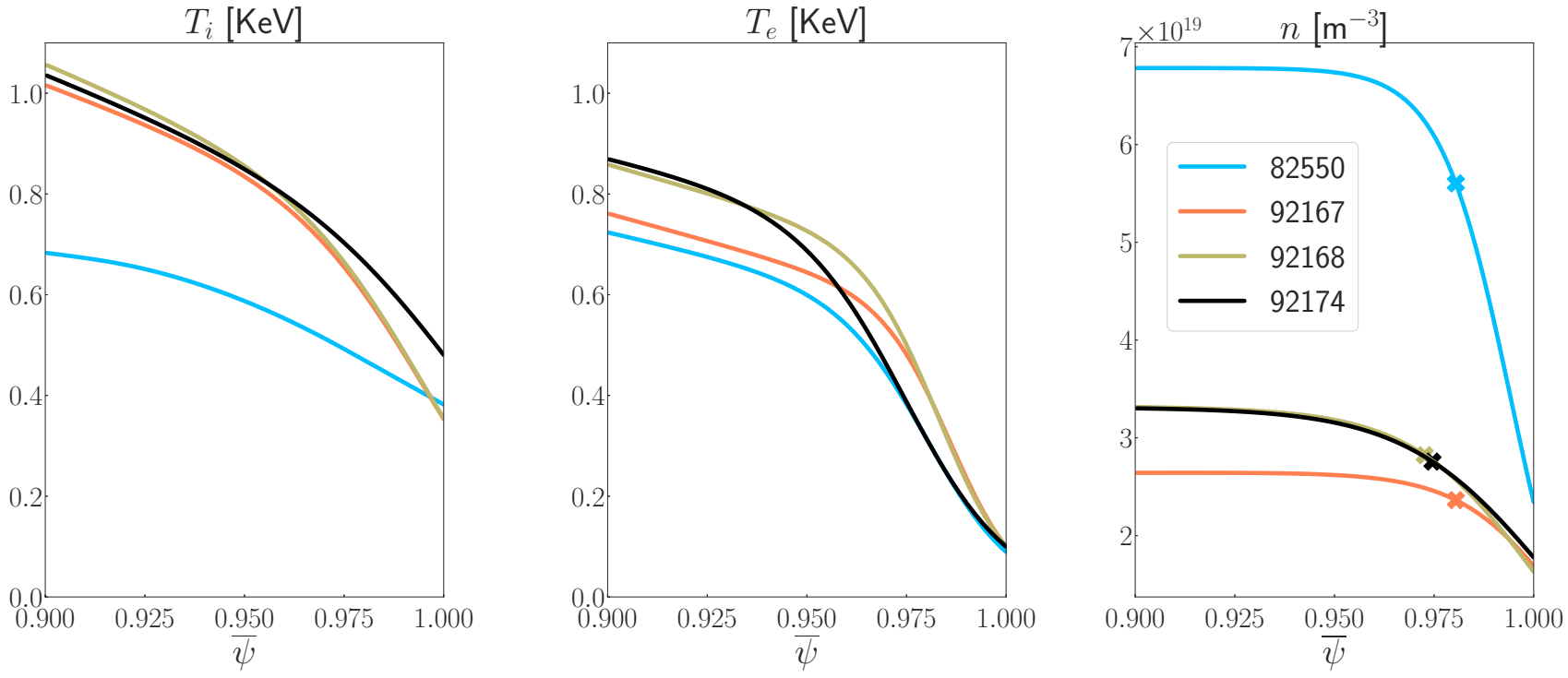

(a) Ion temperature (b) Electron temperature (c) Density

4 JET-ILW Profiles

Equilibrium gradients are much bigger than in the core.

- $R/L_{Te} \approx 50 - 400$, $R/L_{Ti} \approx 30 - 100$. In core, $R/L_{Ts} \approx 5 - 10$. Here R is the major radius, $L_{Ts} \equiv -(\nabla \ln T_s)^{-1}$.

  $\Rightarrow$ dramatic consequences for ETG and ITG(?) stability!

Figure: Temperature and density gradients

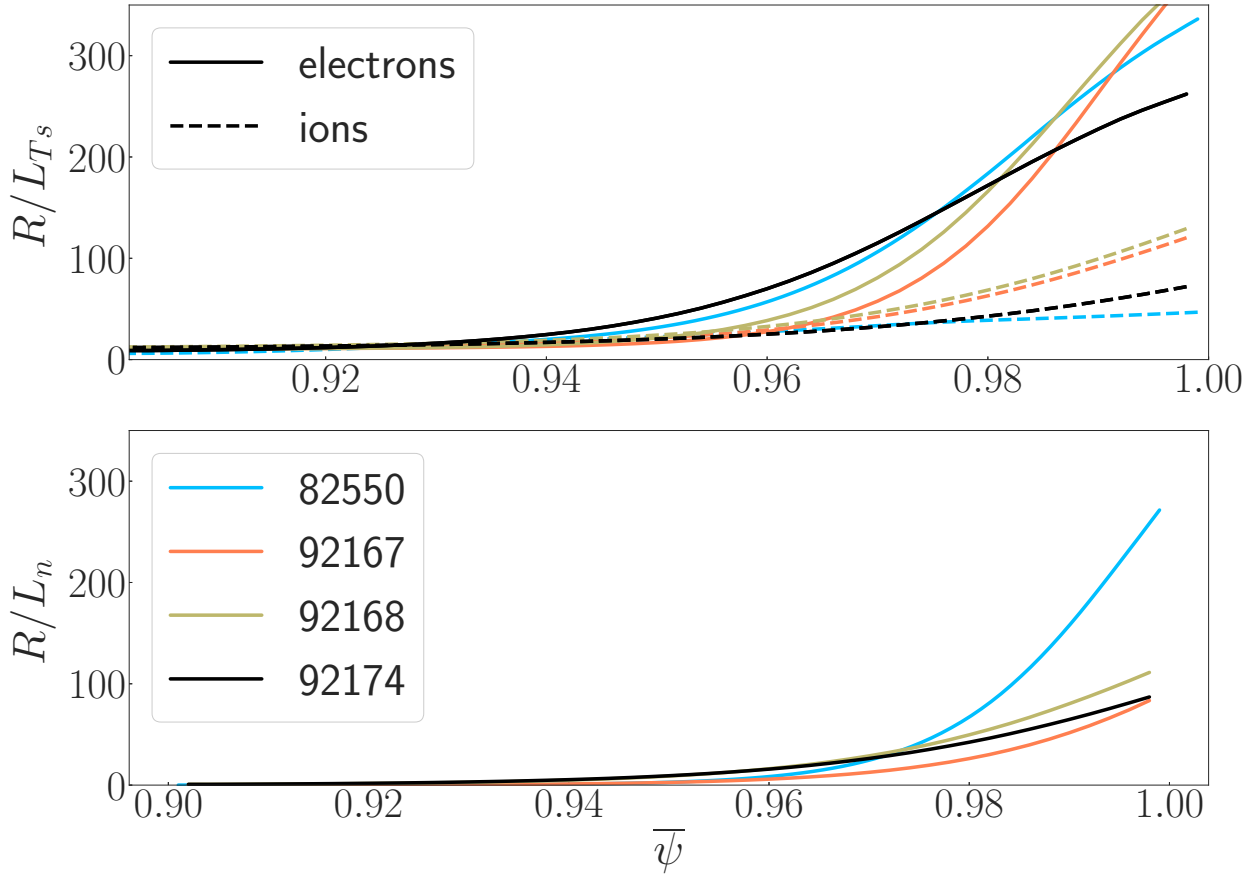

- Use $\{x, y, \theta\}$ real space coordinates: x radial, y field line label.
- Perpendicular perturbation wavenumber, $k_\perp$, with magnetic shear $\hat{s}$,

$$k_\perp \approx \sqrt{k_x^2 + k_y^2} \approx k_y \sqrt{(\hat{s}\theta)^2 + 1}, \tag{1}$$

where $k_x = k_{x0} - k_y \hat{s}\theta$ is an effective radial wavenumber.

- Frequencies, $\omega_{\kappa,s} \equiv \mathbf{k}_\perp \cdot \mathbf{v}_{Ms}$, $\omega_{*e} = \mathbf{v}_E^t \cdot \nabla \ln(n) \frac{T_e}{e\phi^t} = \frac{k_y v_{te} \rho_e}{L_n}$,
where $\mathbf{v}_{Ms} = \frac{1}{\Omega_s}(\hat{\mathbf{b}} \times \nabla \ln \mathbf{B})(v_\parallel^2 + v_\perp^2/2)$ is the magnetic drift.

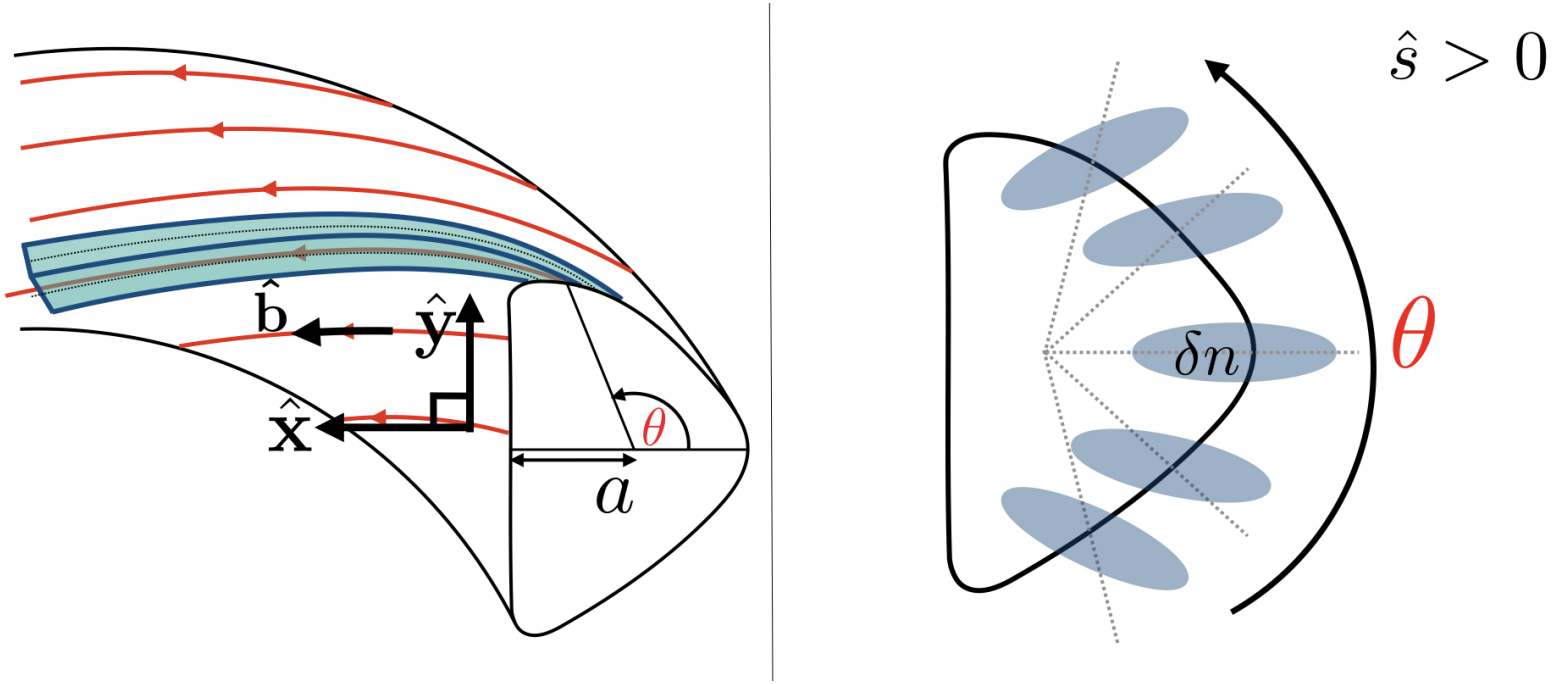

Figure 4: Left: coordinates. Right: magnetic shear acting on perturbation.

Toroidal ETG can be more virulent than expected.

- **Naive** relative size of toroidal and slab drives shows slab dominates, since $k_\parallel$ can become large with k_y for slab,

$$\text{toroidal}: \frac{\omega_{*e}\eta_e}{\omega_{\kappa,e}} \sim \frac{R}{L_{Te}} \gg 1, \quad \text{slab}: \frac{\omega_{*e}\eta_e}{k_\parallel v_{te}} \sim \frac{k_y}{k_\parallel}\frac{\rho_e}{L_{Te}}. \tag{2}$$

  where $\eta_s \equiv L_n/L_{Ts}$.

- **More careful** analysis for toroidal branch shows

$$\text{toroidal}: \frac{\omega_{*e}\eta_e}{\omega_{\kappa,e}} \sim \frac{k_y}{k_\perp}\frac{R}{L_{Te}} \sim \frac{1}{\sqrt{(\hat{s}\theta)^2+1}}\frac{R}{L_{Te}}. \tag{3}$$

  Important! (a): ω_{*e} independent of k_x (b): $k_\perp$ increases along θ due to $\hat{s}$.

- In core, $R/L_{Te} \sim 1$, so dominant toroidal mode at $\theta \sim 0$.
- In pedestal, since $R/L_{Te} \gg 1$, could allow $\hat{s}\theta \gg 1$, and thus toroidal ETG driven at $\hat{s}\theta \gg 1$ ($\rightarrow k_x \gg k_y$), competes with slab ETG.
- Can a toroidal mode find a sufficiently large θ such that it can become large? **We will show it can!**

In pedestal can strongly drive toroidal ETG at $k_y\rho_i \sim 1$ but $k_x\rho_e \sim 1$.

- Figure 5 shows strong toroidal ETG drive at,

$$\frac{\omega_{*e}\eta_e}{\omega_{\kappa,e}} \sim \frac{1}{\sqrt{(\hat{s}\theta)^2+1}}\frac{R}{L_{Te}} \sim 1. \qquad (4)$$

- Thus strong toroidal ETG at

$$\hat{s}\theta \sim \frac{R}{L_{Te}}. \qquad (5)$$

- FLR considerations require $\boxed{k_\perp\rho_e \sim 1}$, FLR damps $k_\perp\rho_e \gg 1$.
- Thus for $\hat{s}\theta \sim R/L_{Te}$,

$$k_\perp\rho_e \sim k_x\rho_e \sim k_y\rho_e\hat{s}\theta \sim 1 \qquad (6)$$

$$\Rightarrow \; k_y\rho_i \sim \sqrt{\frac{m_iT_i}{m_eT_e}}\frac{L_{Te}}{R} \sim 1 \qquad (7)$$

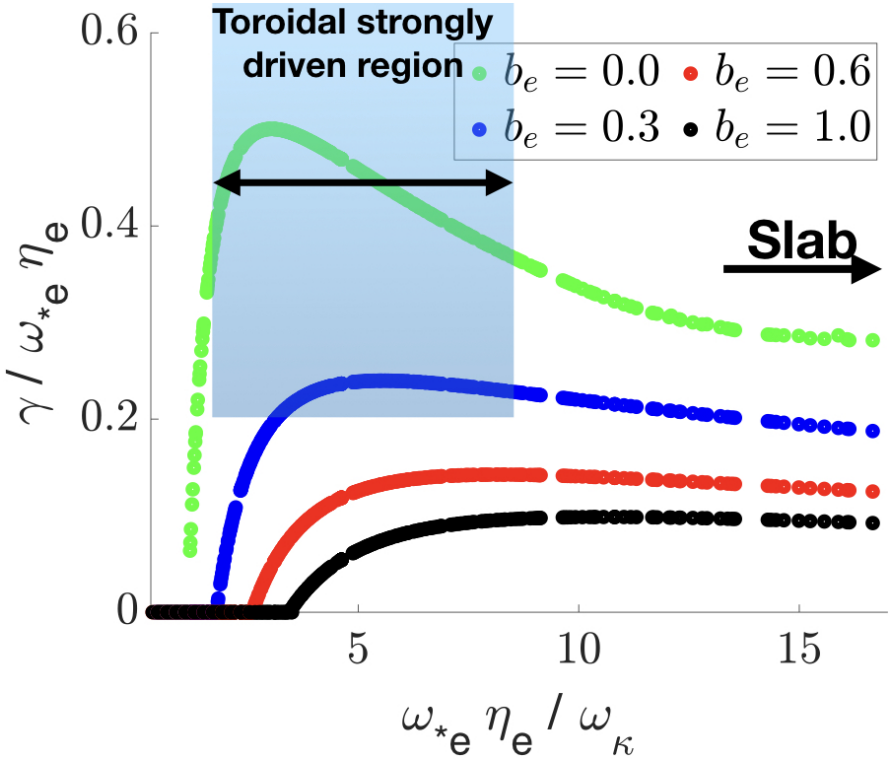

Figure 5: Growth rates for toroidal ETG dispersion relation for $\boxed{b_e = (k_\perp\rho_e)^2/2}$.

- Can show slab ETG driven at $k_y\rho_i \sim \sqrt{m_iT_i/m_eT_e}L_{Te}/R \sim 1$, but $k_x\rho_i \sim 1$.

ITG quenched in JET pedestal simulations, ETG dominant.

- Electrostatic ITG has been named as a dominant transport channel in JET pedestals [Hatch 2016, 2017].
- Similarly can show toroidal ITG strongly driven at $k_y\rho_i \sim L_{Ti}/R \ll 1$, $k_x\rho_i \sim 1$.
- Slab ITG strongly driven at scales as big as $k_y\rho_i \sim L_{Ti}/R \sim k_x\rho_i \ll 1$.
- **However**, in JET-ILW pedestals, often true that $R/L_{Te} \gg R/L_{Ti}$, $\eta_e \gg \eta_i$, might expect ITG to be weak.
- Parameter η_s determines slab stability, mainly R/L_{Ts} for toroidal stability.
- In our JET-ILW simulations, since $\eta_i \sim 1$, slab ITG weak or absent, and R/L_{Ti} too small for toroidal ITG.

  $\Rightarrow$ ITG weak/absent in our pedestal simulations (shown later).

With $R/L_{Ts} \gg 1$, new temperature gradient instability landscape.
(assuming equal ion and electron pressure profiles).

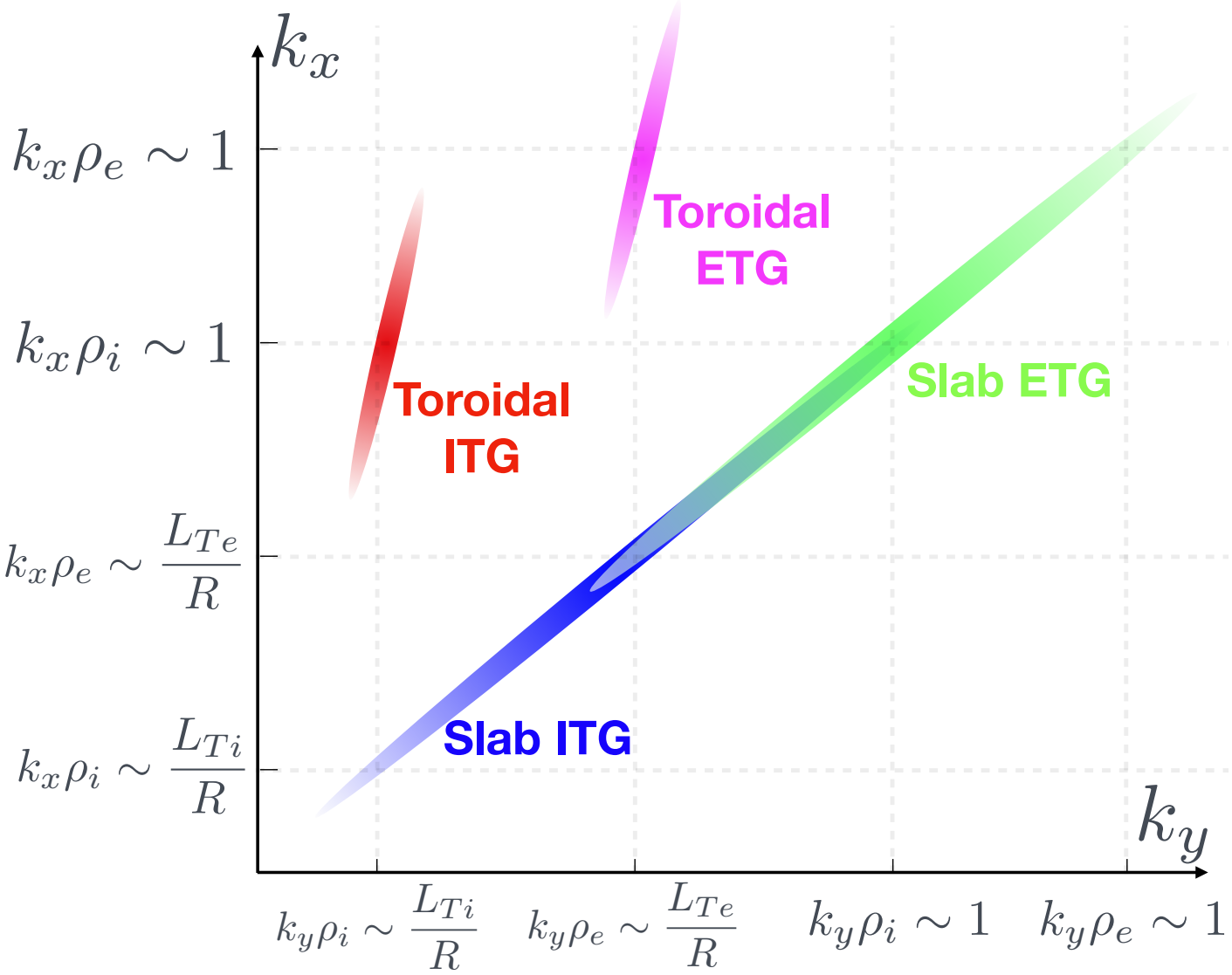

Figure 6: Slab and toroidal temperature gradient instabilities when $R/L_{Ts} \gg 1$. Color indicates locations of instability.

- Linear electrostatic gyrokinetic simulations of JET pedestals to investigate microinstability physics using GS2.
- Simulations carried out at locations marked by crosses.
- $\mathbf{E} \times \mathbf{B}$ shear linearly suppress all electromagnetic modes, motivating electrostatic study.

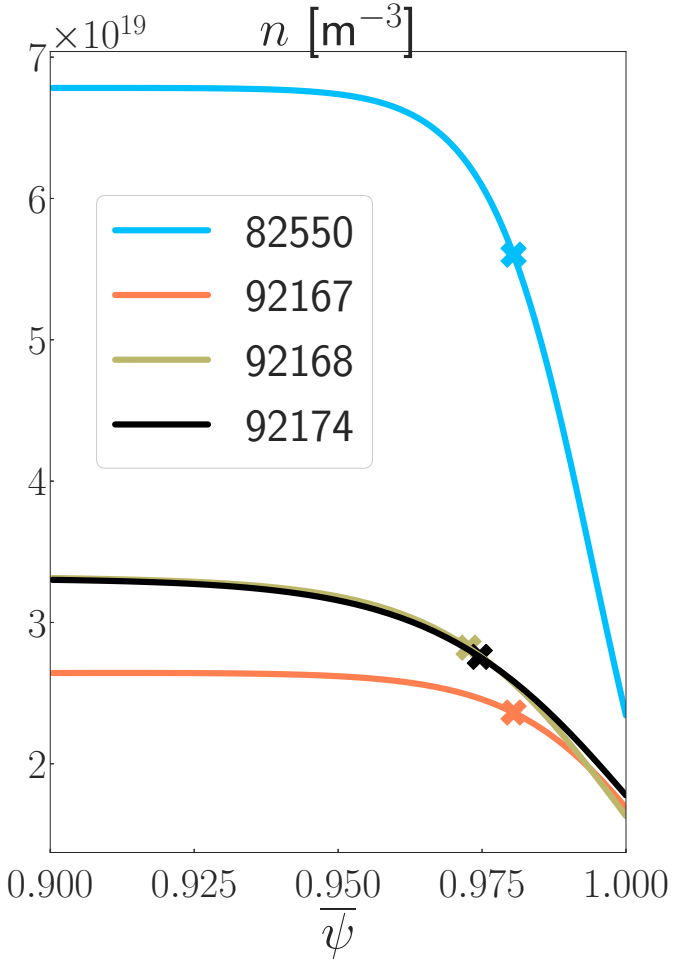

Figure 7: Simulation locations

Kinetic ballooning modes (KBMs) sheared by $\mathbf{E} \times \mathbf{B}$ shear $\Rightarrow$ undergo electrostatic study

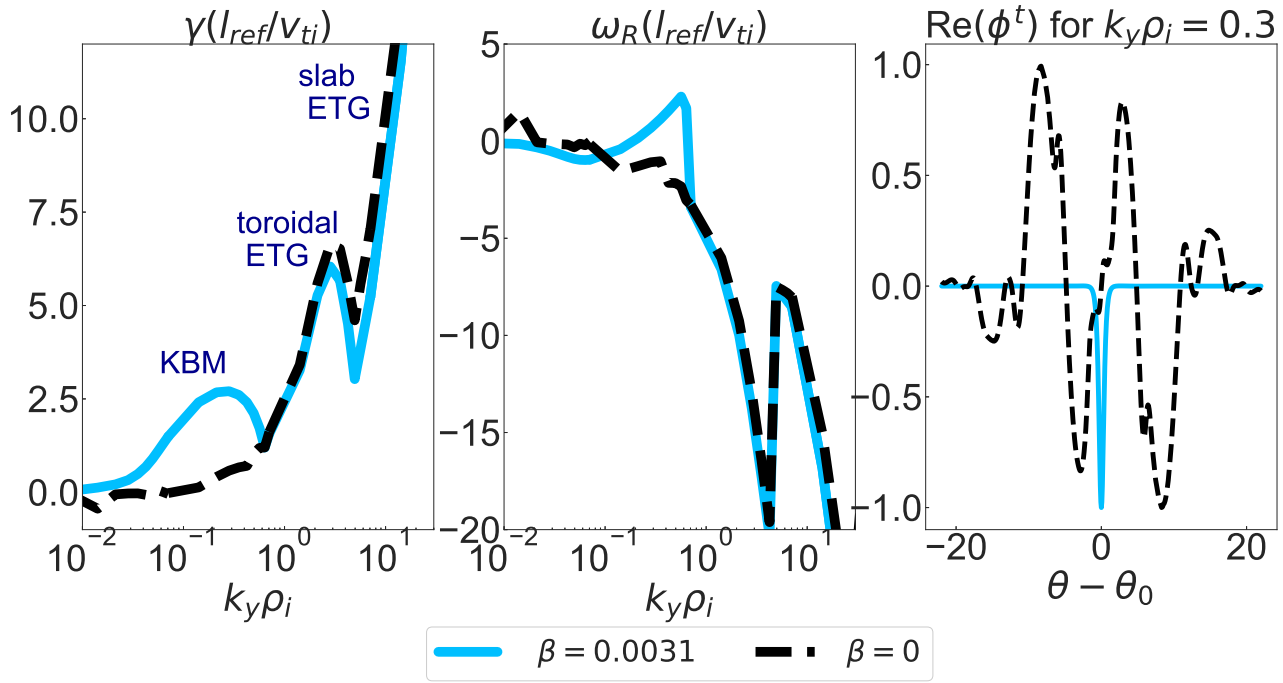

Figure 8: GS2 growth rates (left), real frequencies (middle), eigenmodes (right) for electromagnetic and electrostatic pedestals.

- We investigate instability at each of these scales.
- Most modes propagate in electron diamagnetic direction.
- $\mathbf{E} \times \mathbf{B}$ shear suppresses KBM, rest of spectrum $\approx$ electrostatic.
  $\Rightarrow$ **undergo electrostatic study.**

Gyrokinetic Results ⟩ $1 \lesssim k_y\rho_i \lesssim 5$ Spectra

Modes insensitive to R/L_{Ti}, very sensitive to R/L_{Te}.

- Top: R/L_{Ti} scans. **Toroidal ETG modes completely insensitive to $\mathbf{R/L_{Ti}}$. Even for $R/L_{Ti} \gg R/L_{Te}$, spectrum invariant. Slab modes some $\mathbf{R/L_{Ti}}$ sensitivity.**
- Bottom: $R/L_{Te}, R/L_n$ scans. **Toroidal and slab modes have very strong $\mathbf{R/L_{Te}}$ dependence.** Slab modes also depend on R/L_n.

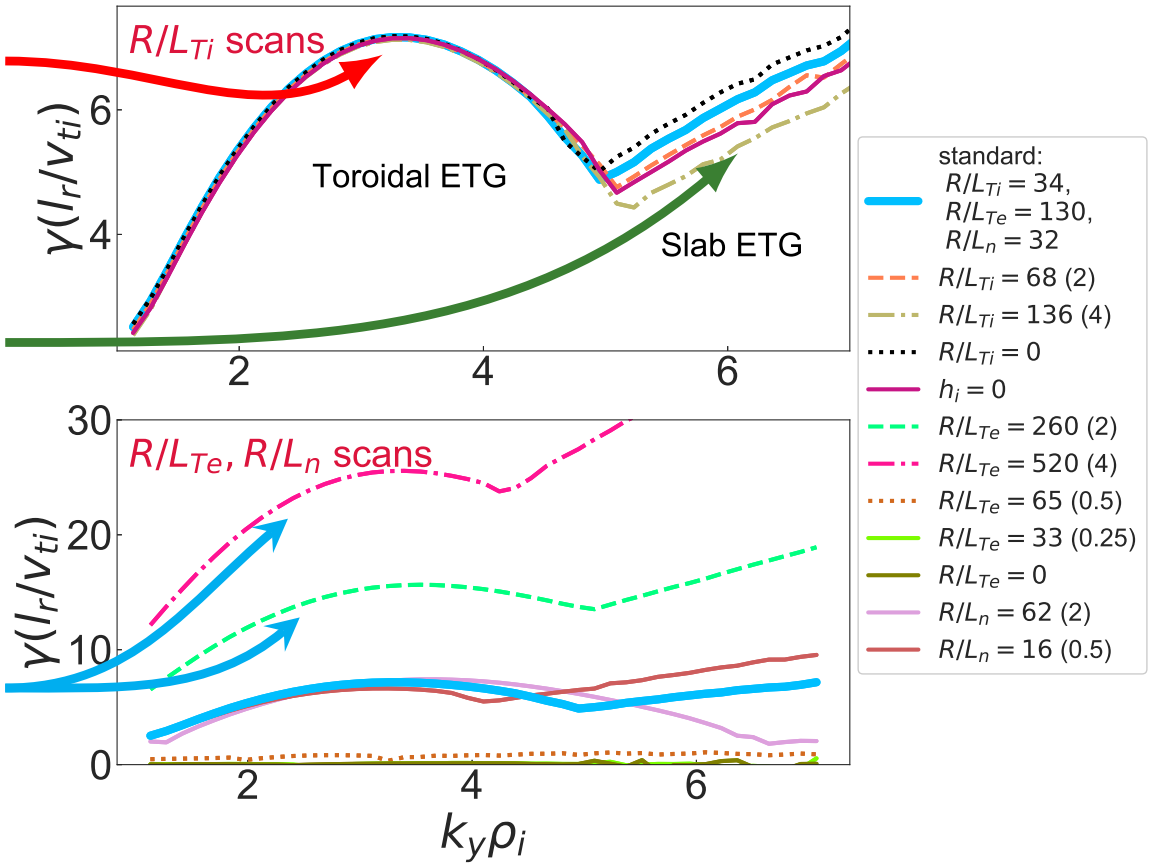

Figure 9: GS2 growth rate spectra.

Gyrokinetic Results ⟩ $1 \lesssim k_y\rho_i \lesssim 5$ Eigenmodes

Toroidal ETG eigenmodes localized at large θ.

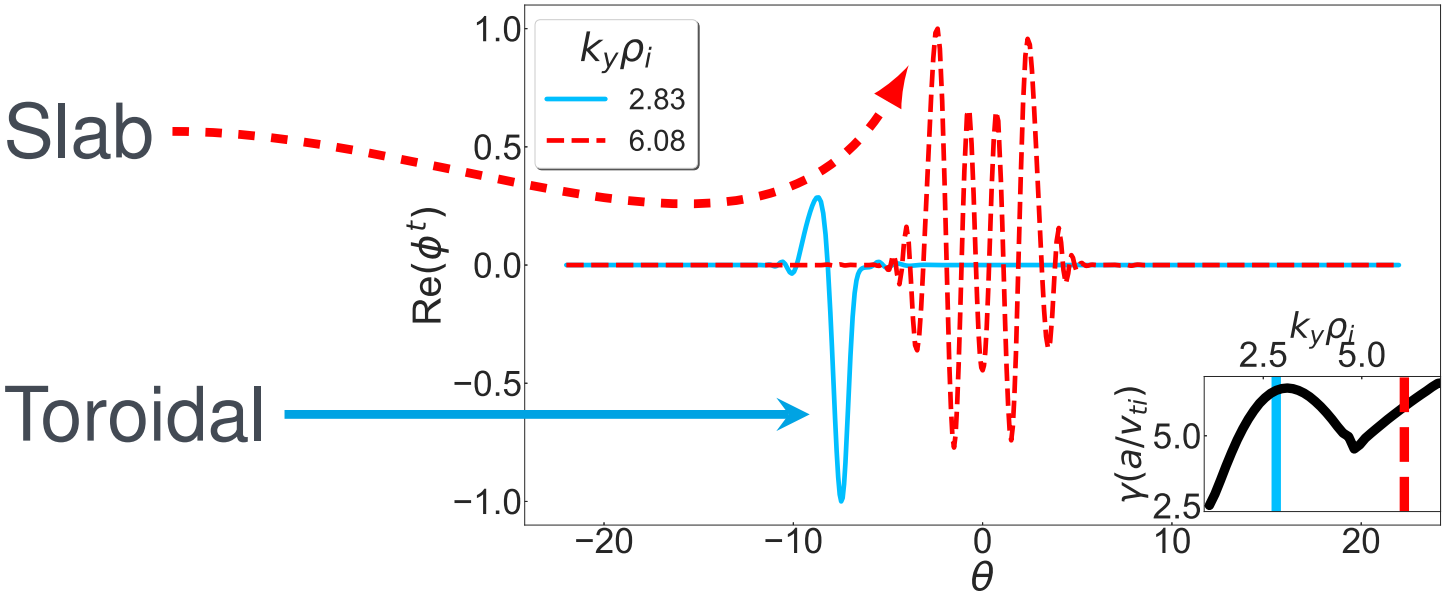

Figure 10: GS2 eigenmodes for toroidal (blue) and slab (red) ETG.

- Toroidal ETG driven at $\hat{s}\theta \gg 1$.
- Do not see toroidally localized ETG in core because $R/L_{Te} \sim 1$ in core, thus core toroidal modes less localized.
- Toroidal ETG eigenmodes choose θ location based on combination of FLR effects and magnetic drifts ($\omega_{*e}\eta_e \sim \omega_{\kappa,e}$).

Magnetic shear ineffective at reducing toroidal ETG growth rate.

- If $\hat{s}$ changes, mode can move in θ to keep growth rate large,

$$\frac{\omega_{*e}\eta_e}{\omega_{\kappa,e}} \sim \frac{1}{\hat{s}\theta}\frac{R}{L_{Te}} \sim 1.$$

- Only for $\hat{s}$ very large will toroidal mode be forced to a small $|\theta| \approx 0 \rightarrow$ growth rate will decrease as $\hat{s}$ increases when $|\theta| \approx 0$.

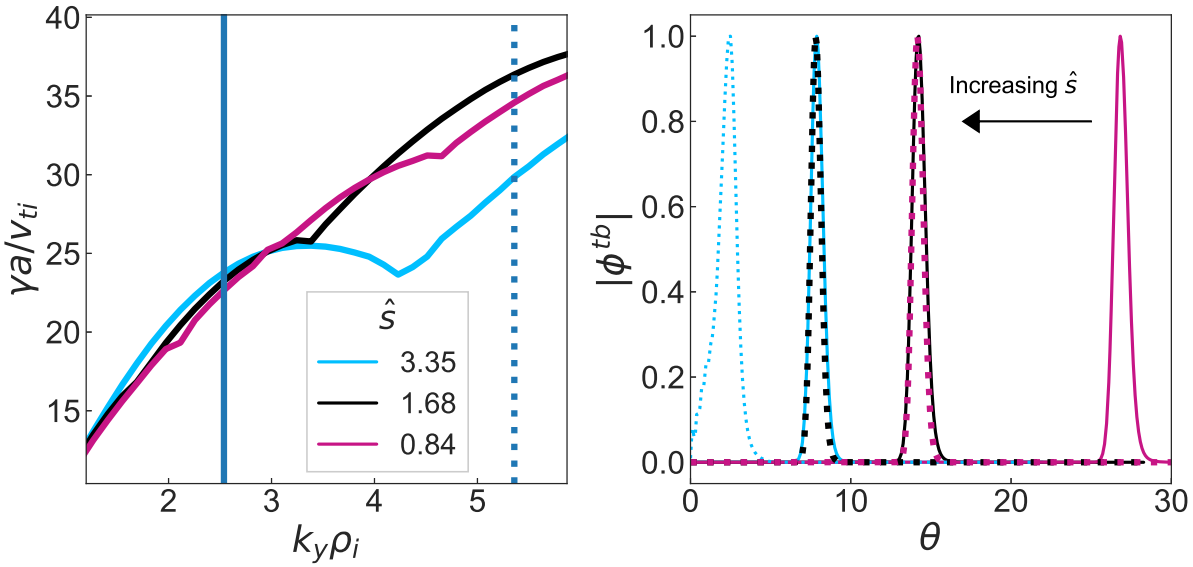

Figure 11: GS2 Linear spectra (left) and eigenmodes (right) for different $\hat{s}$ values.

FLR effects strongly determine the θ location for toroidal ETG.

- Mode has maximum amplitude very close to a local minimum in $k_\perp$, as shown below, where $\Gamma_0(b_e) = I_0(b_e)\exp(-b_e)$ and $b_e = (k_\perp \rho_e)^2/2$.

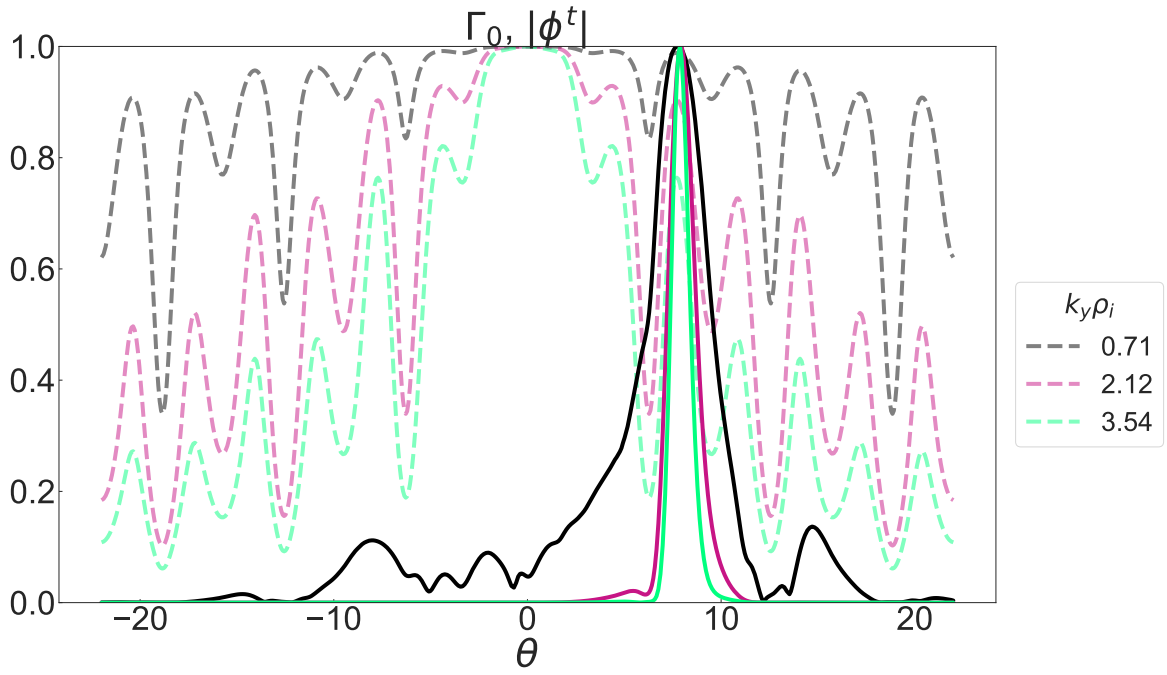

Figure 12: GS2 eigenmodes (solid) and $\Gamma_0(b_e)$ for three separate k_y values.

Pedestal toroidal ETG modes sit at local minima in $k_\perp$ where FLR effects are locally (in θ) smallest.

- Local magnetic shear causes local minima in $k_\perp$, which is where the mode's maximum amplitude (roughly) sits.

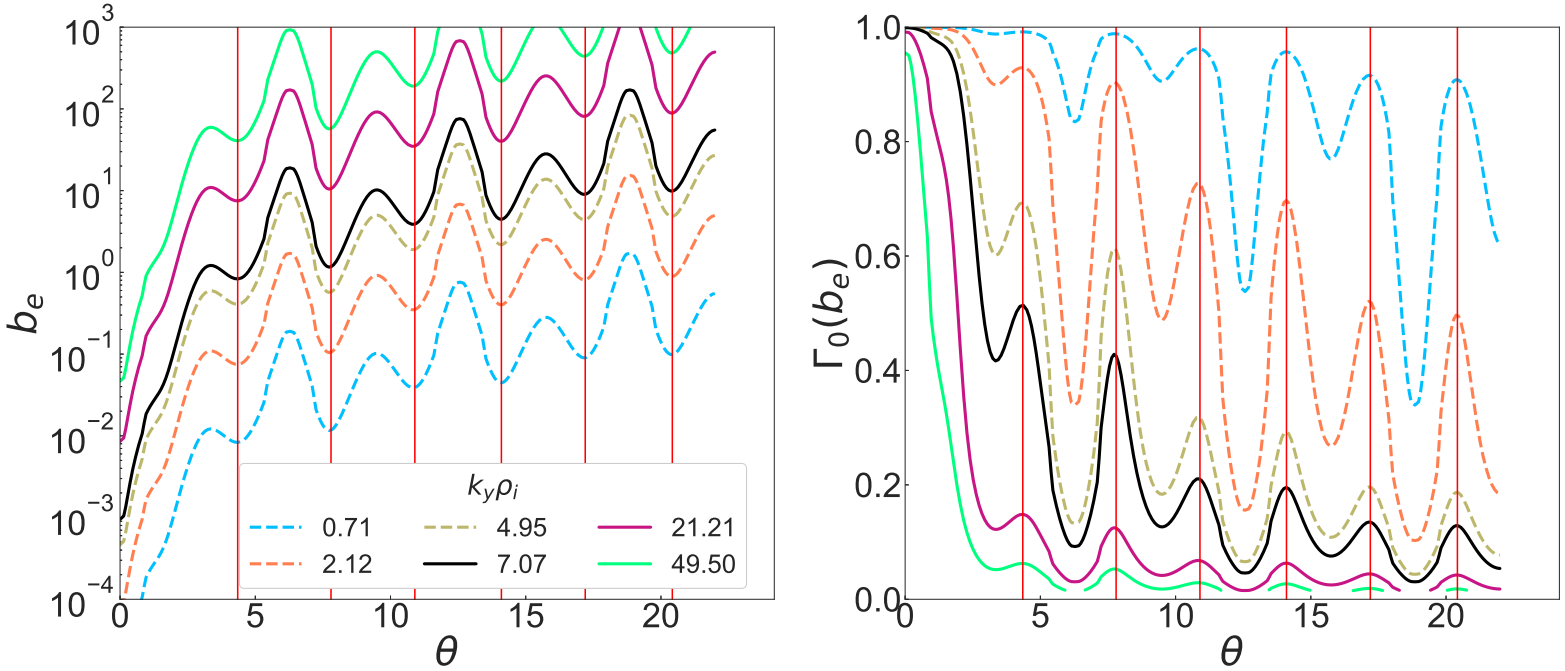

Figure 13: The value b_e along a field line (left) and associated $\Gamma_0(b_e)$ (right) for different $k_y\rho_i$ values. Local minima of $k_\perp$ denoted by vertical lines.

Modes move in θ as $k_y\rho_e$ increases. Relative sign of ω_{*e} and $\omega_{\kappa,e}$ determine the θ domain..

- Using $k_\perp \sim 1/\rho_e$, one finds

$$\frac{\omega_{*e}\eta_e}{\omega_{\kappa,e}} \sim k_y\rho_e\frac{R}{L_{Te}} \sim k_y\rho_e\hat{s}\theta. \tag{8}$$

- In $k_\parallel v_{te} \ll \omega$, $b_e \ll 1$ limit, $\omega_{*e}\omega_{\kappa,e}\eta_e > 0$ for instability [Biglari, 1989].

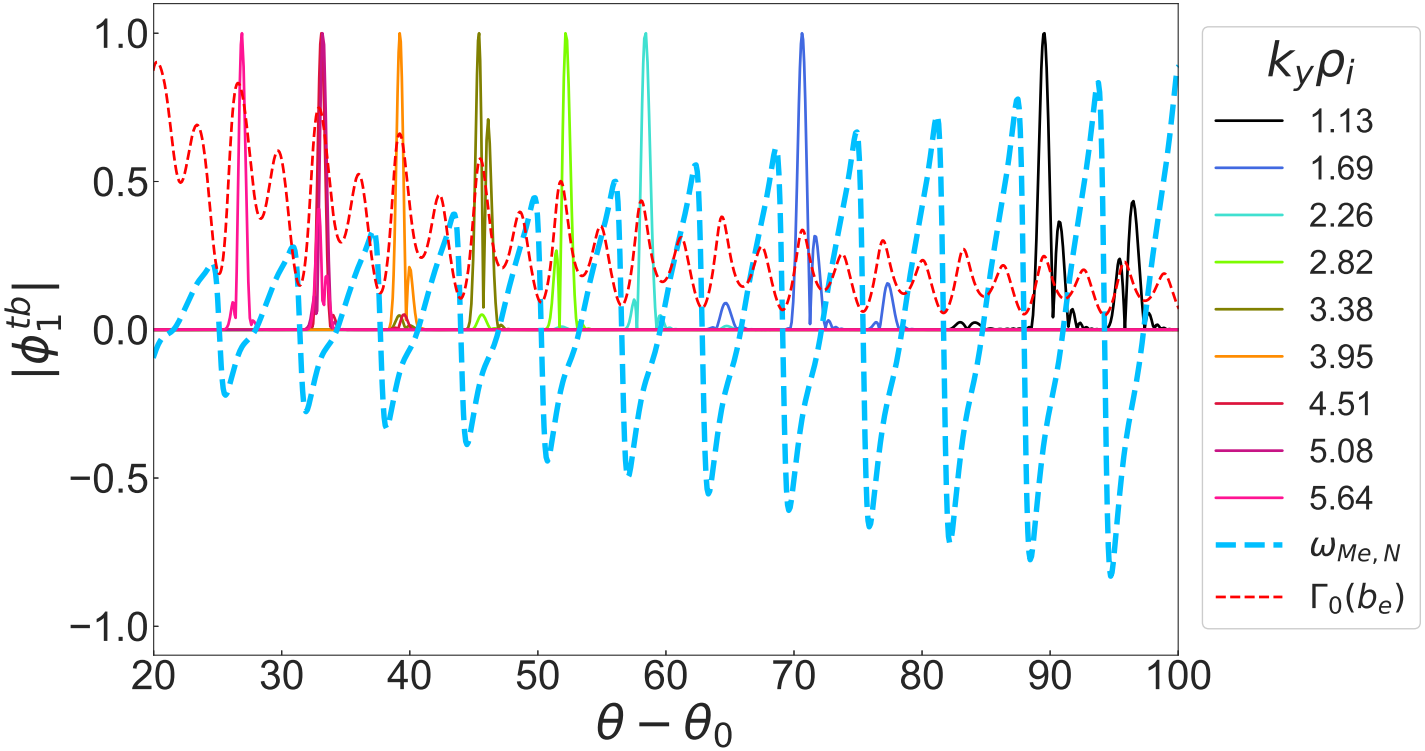

Figure 14: GS2 eigenmodes moving to smaller θ due to increasing $k_y\rho_e$. Here, $\hat{s}$ and L_{Te}/R are four times smaller to make eigenmodes more mobile in θ.

The relative signs of ω_{*e} and $\omega_{\kappa,e}$ determine the θ domain.

- Flipping sign of $\omega_{\kappa,e}$ makes toroidal ETG mode jump to where $\omega_{*e}\omega_{\kappa,e}\eta_e > 0$.

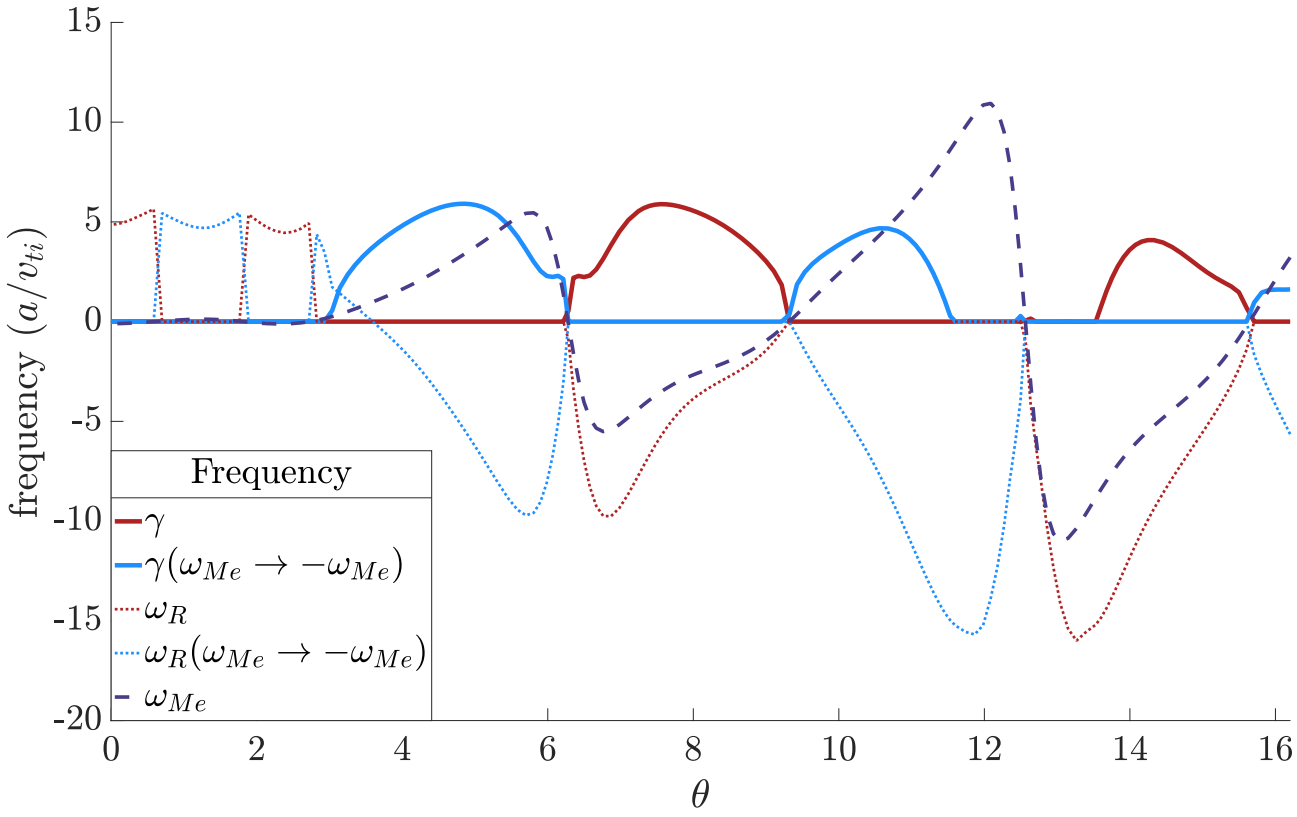

Figure 15: Linear growth rates versus θ for analytic dispersion relation, with $k_{\|} = 0$.

Theory describes toroidal and slab ETG well.

- Local gyrokinetic dispersion relation describes toroidal and slab ETG surprisingly well.
- Finding $k_{\|}$ for toroidal ETG modes still not solved.

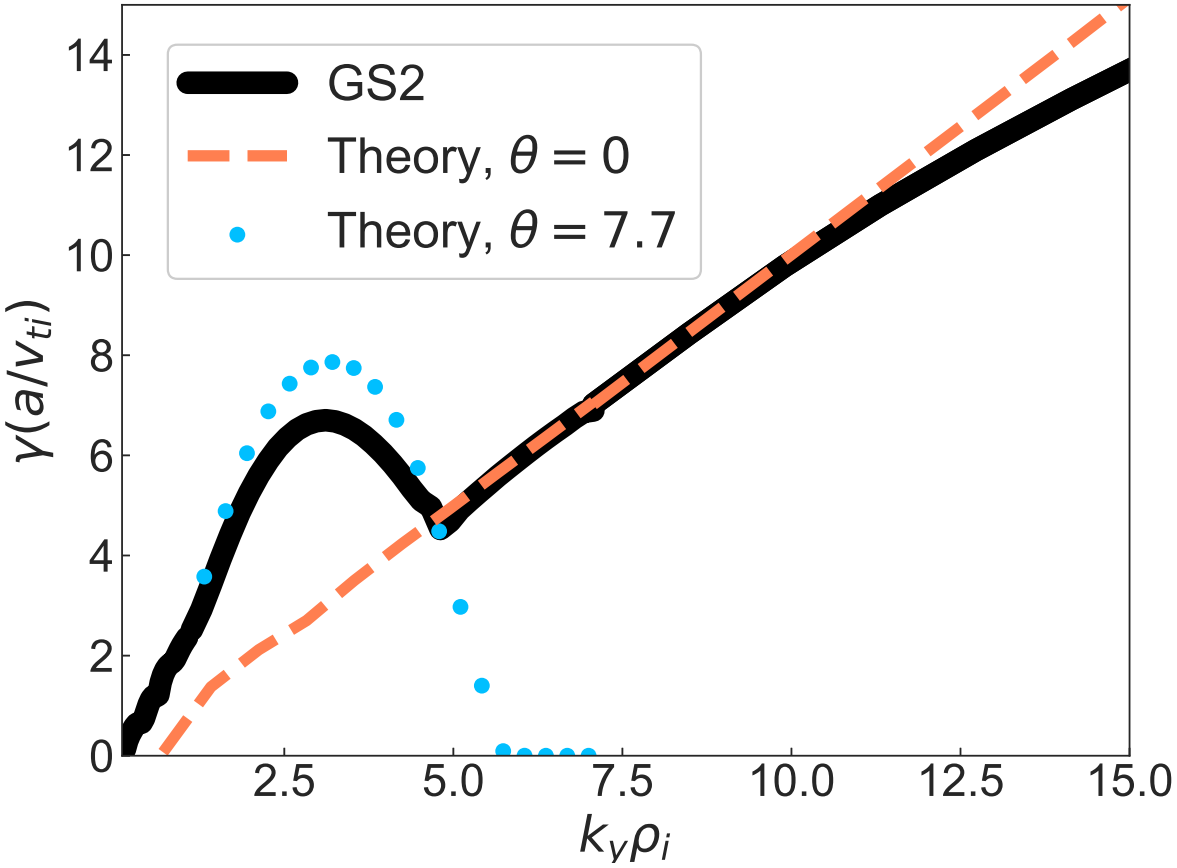

Figure 16: Linear growth rates from GS2 versus solutions to gyrokinetic dispersion relation.

Measured T_i profiles have stable ITG at all scales.

- We expect to drive strong slab and toroidal ITG at $k_y\rho_i \sim L_{Ti}/R \ll 1$.
- However, we are unable to find ITG with measured profiles.

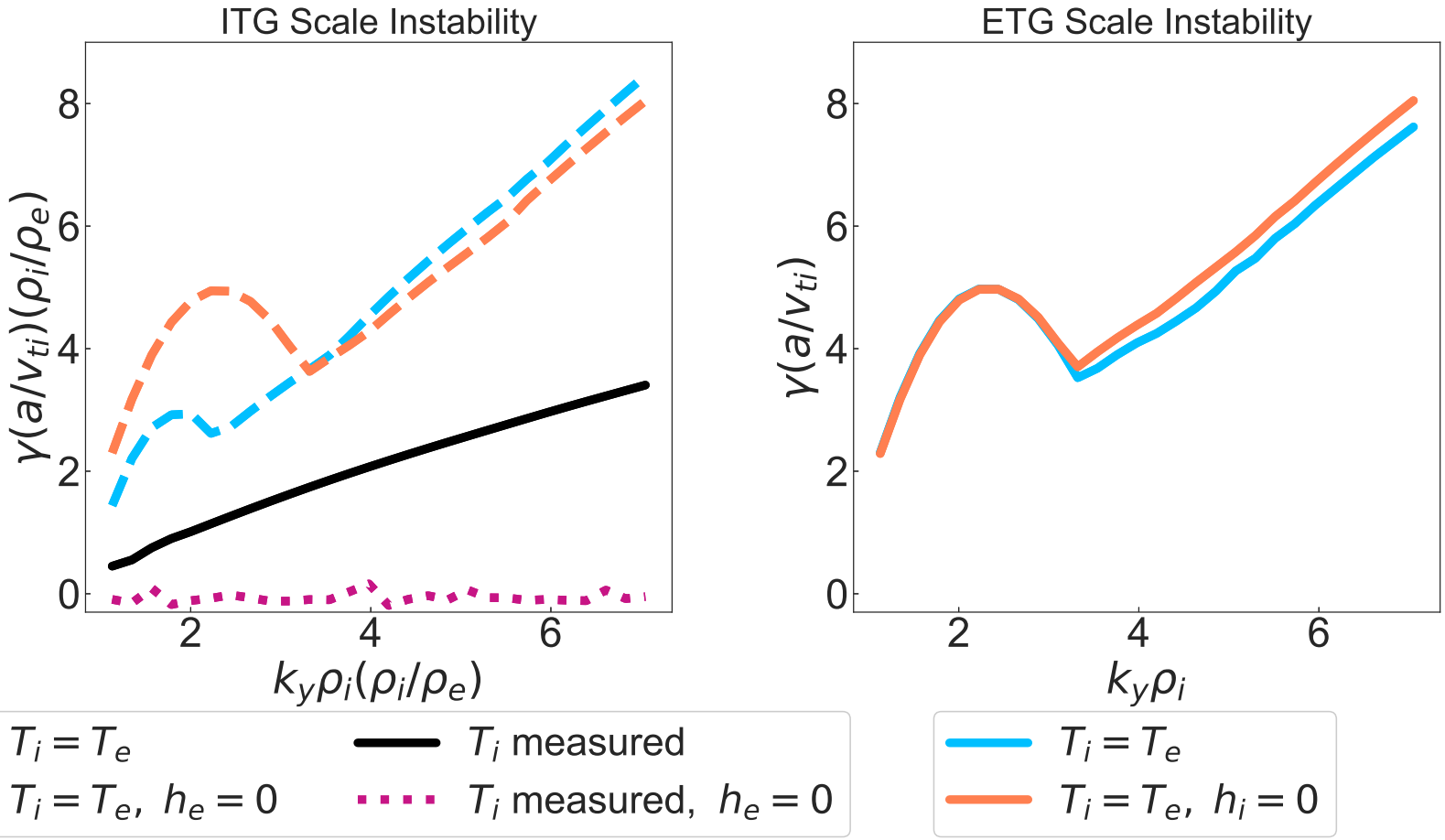

Figure 17: Spectra at $k_y\rho_i \ll 1$ (left) and $k_y\rho_i \sim 1$ (right). Electron modes are solid, ion modes are dashed.

Summary 〉 Findings

- Toroidal ETG is driven at $k_y\rho_i \sim 1$ but $k_x\rho_e \sim 1$, because $R/L_{Te} \gg 1$.
- Slab ETG driven at scales as large as $k_y\rho_i \sim k_x\rho_i \sim 1$, because $R/L_{Te} \gg 1$.
- $\mathbf{E} \times \mathbf{B}$ shear suppresses KBMs, ITG in JET pedestals we investigated.
- Modes at all scales are most sensitive to electron temperature gradient physics.
- Local dispersion relation describes toroidal and slab ETG well.
- Linearly, ITG is highly subdominant/absent because $\eta_i \sim 1$, R/L_{Ti} below critical value.

Items I haven't covered, but would be very happy to discuss this week:

- Effects of θ_0 on linear toroidal ETG (*nearly solved*).
- Linear stability calculation for toroidal ETG with general $k_{\|}$ and full FLR effects (*nearly solved*).
- Effects of ions on slab ETG (*partly solved*).
- Nonlinear results (hard because multiscale, how important are these toroidal ETG modes?) (*unsolved*).
- Finding $k_{\|}$ self-consistently for toroidal modes (*unsolved*).
- Modes at $k_y \rho_i \lesssim 1$ (perhaps more transport relevant) (*unsolved*).

We gratefully acknowledge useful conversations with T. Adkins, J. R. Ball, N. Christen, W. Dorland, M. R. Hardman, D. Hatch, W. Guttenfelder, Y. Kawazura, J. C. Hillesheim, A. Mauriya, S. Saarelma, and A. A. Schekochihin. JFP is supported by EPSRC Scholarship No 3000207032. FIP, MB, and CMR are supported in part by the RCUK Energy-Programme (grant number EP/EPI501045). PGI is supported by an EU H2020 grant, agreement No 3000207035. Computational time provided by Plasma HEC Consortium EPSRC (grant number EP/L000237/1). This work has been carried out within the framework of the EUROfusion Consortium and has received funding from the Euratom research and training programme 2014-2018 under grant agreement No 633053 and from the RCUK Energy Programme (grant number EP/P012450/1). JFP acknowledges travel support from Merton College, Oxford.

$$\mathbf{k}_\perp = k_x \nabla x + k_y \nabla y = \left[k_x - k_y\left(\hat{s}\theta - \frac{r}{q_c}\frac{\partial \nu}{\partial r}\right)\right]\nabla x \tag{9}$$

$$+ \frac{\partial \psi}{\partial r}\frac{1}{B_a} k_y \left[\nabla \zeta + \left(\frac{\partial \nu}{\partial \theta} - q\right)\nabla \theta\right], \tag{10}$$

using

$$\alpha = \zeta - q(x)\theta + \nu(x, y), \tag{11}$$

and the effective radial wavenumber is

$$k_x = k_{x0} - k_y\left(\hat{s}\theta - \frac{r}{q_c}\frac{\partial \nu}{\partial r}\right). \tag{12}$$

From quasineutrality, the electrostatic dispersion relation is,

$$Z_i \frac{T_{0e}}{T_{0i}} + 1 - \sum_s D_s = 0, \tag{13}$$

where

$$D_s = iZ_s^2 \frac{T_{0e} n_{0s}}{T_{0s} n_{0e}} \int_0^\infty d\lambda \frac{\Gamma_0(\hat{b}_s^\sigma)}{(1+i\sigma\lambda)^{1/2}(1+i\sigma\lambda/2)} \exp\left(i\lambda\widehat{\omega}\right) \exp\left(-\frac{(\lambda\widehat{k}_{\|})^2}{4(1+i\sigma\lambda)}\right)$$
$$\left[-\widehat{\omega} + \widehat{\omega}_{*s}\left(1 + \eta_s\left\{\frac{2(1+i\sigma\lambda) - (\widehat{k}_{\|}\lambda)^2}{4(1+i\sigma\lambda)^2}\right.\right.\right.$$
$$\left.\left.\left. + \frac{1}{(1+i\sigma\lambda/2)} - \hat{b}_s^\sigma \frac{1 - \Gamma_1(\hat{b}_s^\sigma)/\Gamma_0(\hat{b}_s^\sigma)}{(1+i\sigma\lambda/2)} - \frac{3}{2}\right\}\right)\right].$$

This is not a straightforward integral for $\gamma = 0$.

With

$$\frac{\mathbf{k}_\perp \cdot \mathbf{v}_{Mi}}{\omega} \sim \frac{(k_\parallel v_{ti})^2}{\omega^2}, \quad \omega \gg k_\parallel v_{ti}, \tag{14}$$

$$1 + \frac{ZT_e}{T_i}\left(1 - \frac{\omega_{*i}}{\omega} - \frac{\omega_{*i} k_\parallel^2 \eta_i T_i}{\omega^3 m_i} - \frac{\omega_{*i}\omega_{\kappa,i}\eta_i}{\omega^2}\right) = 0, \tag{15}$$

which for $k_\parallel = 0$, gives

$$\omega = 0, \quad \omega = \frac{\omega_{*i}}{2\left(1 + \frac{Z_i T_e}{T_i}\right)} \pm \sqrt{\frac{\omega_{*i}^2}{4\left(1 + \frac{Z_i T_e}{T_i}\right)^2} + \frac{\omega_{*i}\omega_{\kappa,i}\eta_i}{\left(1 + \frac{Z_i T_e}{T_i}\right)^2}}. \tag{16}$$

In GS2land, $\omega_{*e} < 0$.

With $R/L_n \gg 1$,

$$\gamma \sim \pm\eta_e \frac{\omega_\pm}{\omega_{*e}} \frac{R}{L_n}, \tag{17}$$

where

$$\omega_\pm = \pm\frac{\omega_{*e}}{2}\left(1 + \sqrt{1 - 8\frac{L_n}{R}\eta_i\frac{T_i}{T_e}}\right). \tag{18}$$

$\mathbf{E} \times \mathbf{B}$ shear suppresses KBMs, ITG, but not ETG.

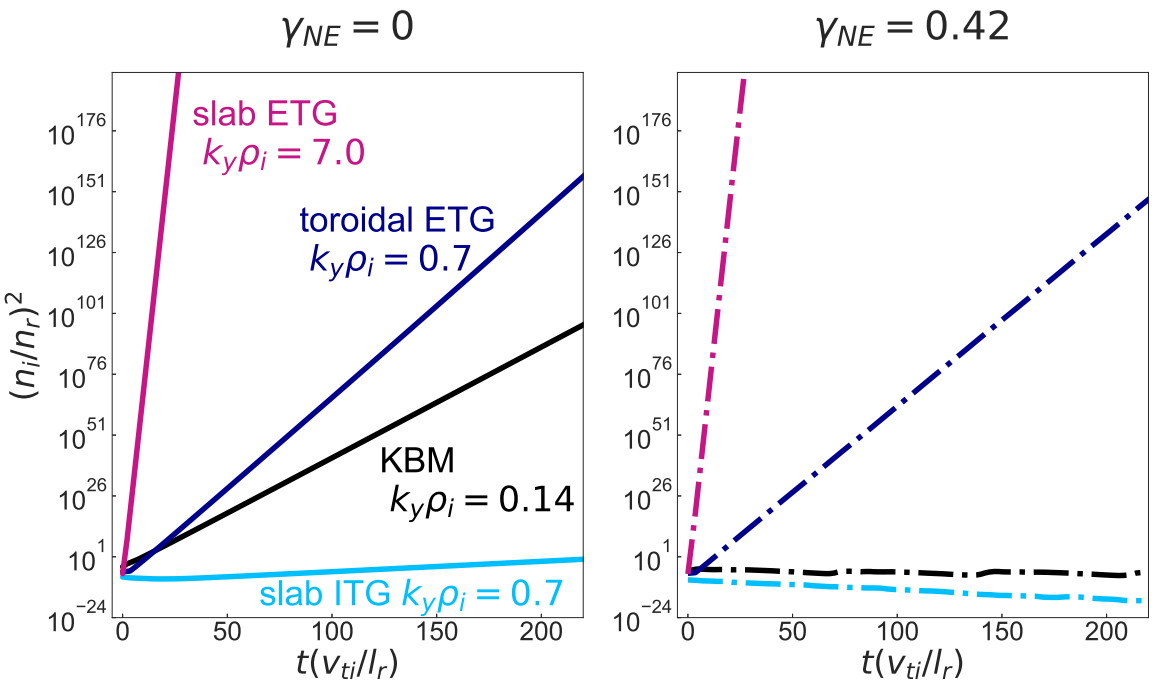

Figure 18: Effect of $\mathbf{E} \times \mathbf{B}$ shear on different modes.

- KBMs and ITG easily suppressed by $\mathbf{E} \times \mathbf{B}$ shear.
- ETG very resistant to $\mathbf{E} \times \mathbf{B}$ shear.

Eigenmodes Extended in θ.

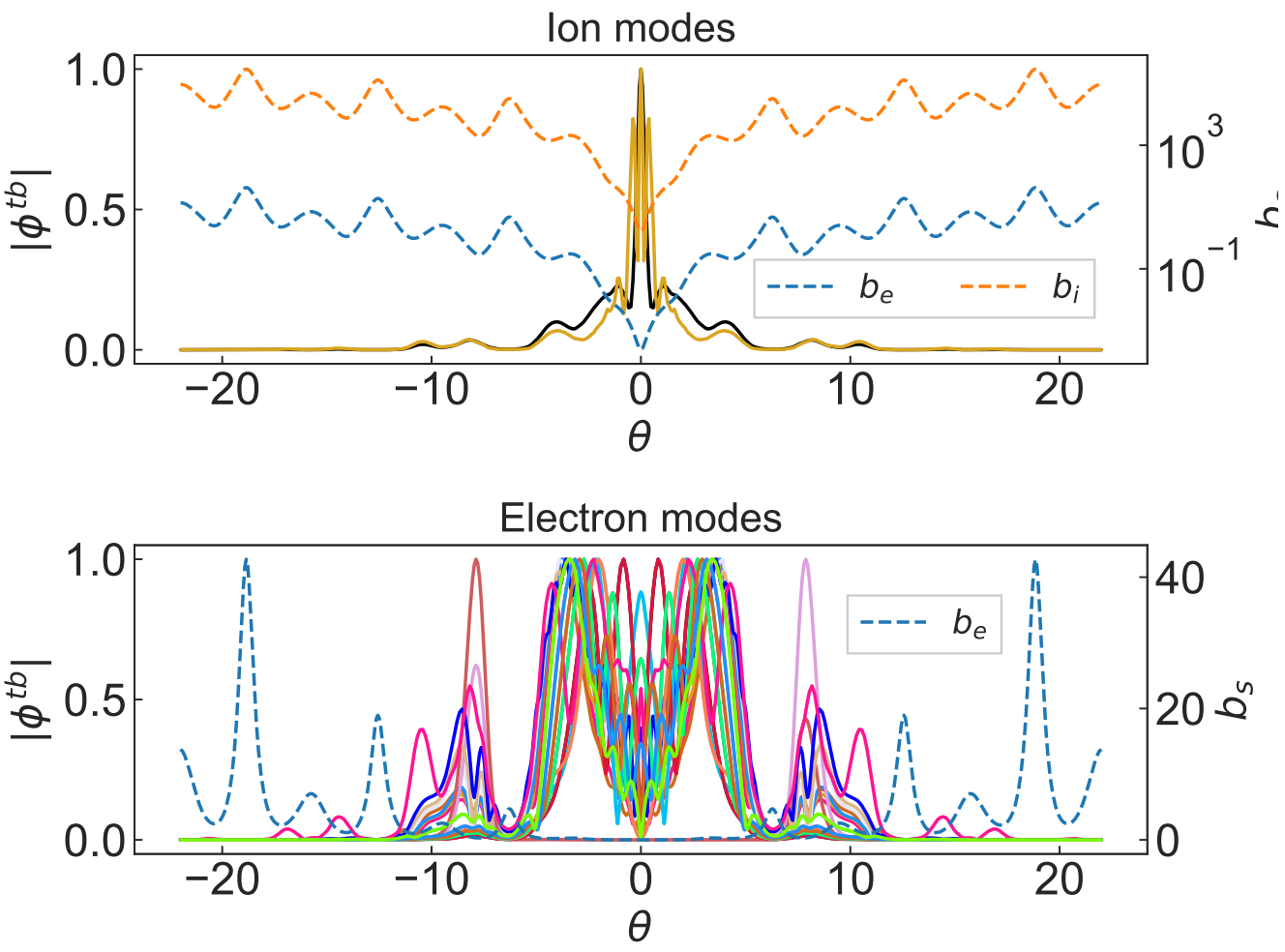

Figure 19: Electron and ion direction eigenmodes obtained using GS2 eigensolver at $k_y\rho_i = 3.5$.

ITG has very low growth rates in our pedestals.

- Using GS2 eigensolver mode, we find a single very weak ITG-like mode at $k_y\rho_i = 3.5$, from two modes in the ω_{*i} direction.
- For this ITG mode, $\gamma a/v_{ti} = 0.07$, whereas for the fastest growing ETG mode at $k_y\rho_i = 3.5$ has $\gamma a/v_{ti} = 7.1$.

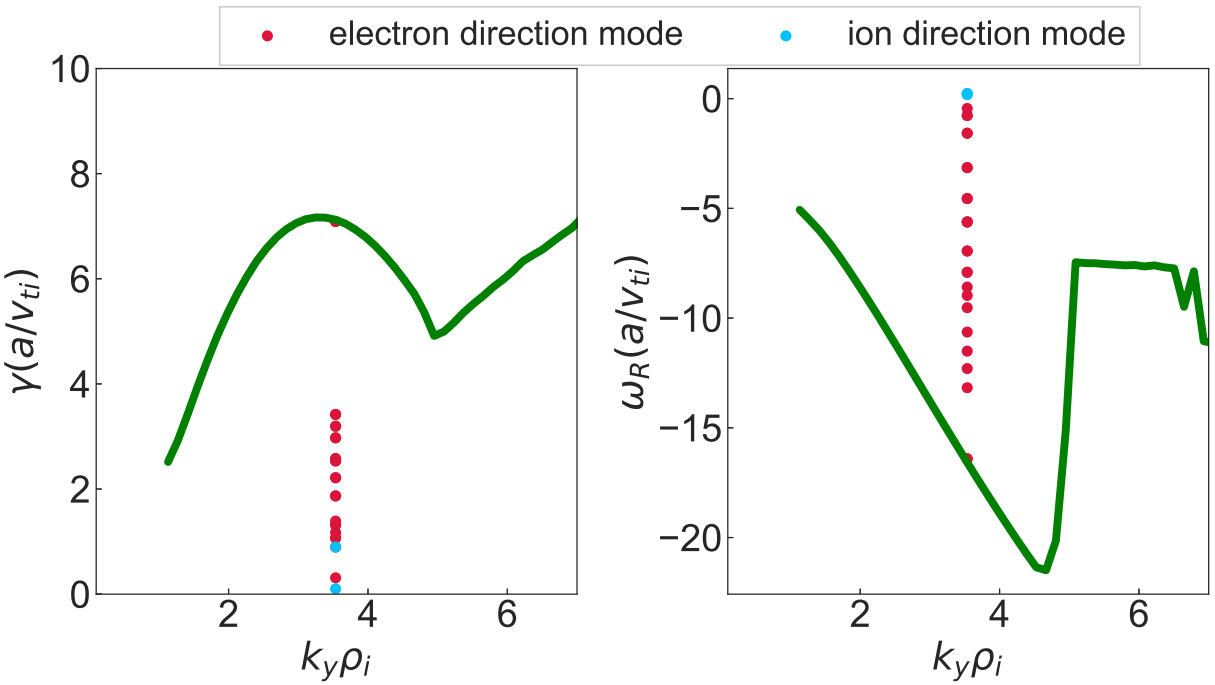

Figure 20: Imaginary (left) and real (right) frequencies for the 17 eigenmodes found at $k_y\rho_i = 3.5$.

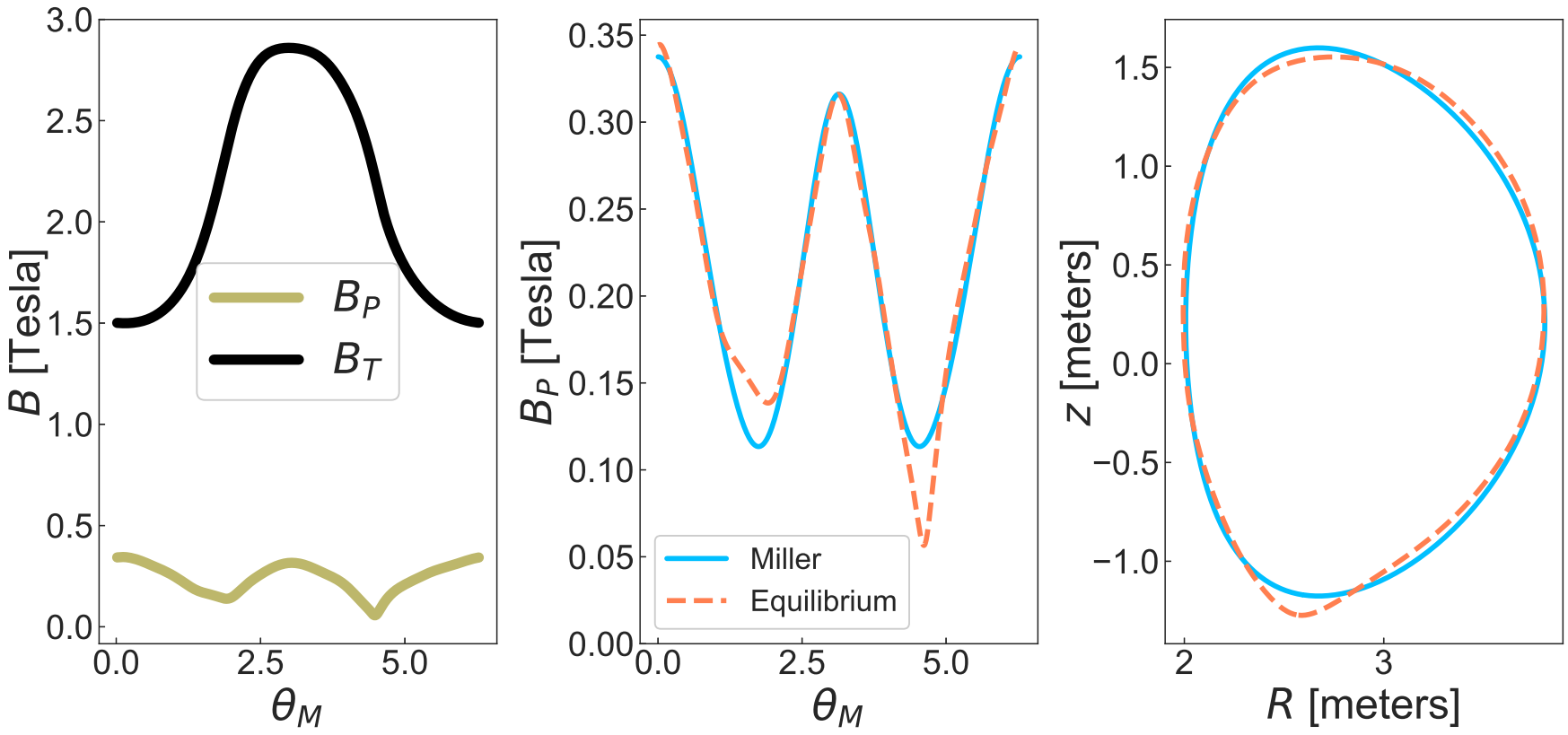

Figure 21: Miller equilibrium for JET shot 92174.